JCI The Journal of Clinical Investigation

Cardiotoxicity of doxorubicin is mediated through mitochondrial iron accumulation

Yoshihiko Ichikawa, … , Tejaswitha Jairaj Naik, Hossein Ardehali

J Clin Invest. 2014;124(2):617-630. https://doi.org/10.1172/JCI72931.

Research Article **Cardiology**

Doxorubicin is an effective anticancer drug with known cardiotoxic side effects. It has been hypothesized that doxorubicin-dependent cardiotoxicity occurs through ROS production and possibly cellular iron accumulation. Here, we found that cardiotoxicity develops through the preferential accumulation of iron inside the mitochondria following doxorubicin treatment. In isolated cardiomyocytes, doxorubicin became concentrated in the mitochondria and increased both mitochondrial iron and cellular ROS levels. Overexpression of ABCB8, a mitochondrial protein that facilitates iron export, in vitro and in the hearts of transgenic mice decreased mitochondrial iron and cellular ROS and protected against doxorubicin-induced cardiomyopathy. Dexrazoxane, a drug that attenuates doxorubicin-induced cardiotoxicity, decreased mitochondrial iron levels and reversed doxorubicin-induced cardiac damage. Finally, hearts from patients with doxorubicin-induced cardiomyopathy had markedly higher mitochondrial iron levels than hearts from patients with other types of cardiomyopathies or normal cardiac function. These results suggest that the cardiotoxic effects of doxorubicin develop from mitochondrial iron accumulation and that reducing mitochondrial iron levels protects against doxorubicin-induced cardiomyopathy.

Cardiotoxicity of doxorubicin is mediated through mitochondrial iron accumulation

Yoshihiko Ichikawa,[1] Mohsen Ghanefar,[1] Marina Bayeva,[1] Rongxue Wu,[1] Arineh Khechaduri,[1] Sathyamangla V. Naga Prasad,[2] R. Kannan Mutharasan,[1] Tejaswitha Jairaj Naik,[1] and Hossein Ardehali[1]

[1]Feinberg Cardiovascular Institute, Northwestern University School of Medicine, Chicago, Illinois, USA.
[2]Department of Molecular Cardiology, Lerner Research Institute, Cleveland Clinic Foundation, Cleveland, Ohio, USA.

Doxorubicin is an effective anticancer drug with known cardiotoxic side effects. It has been hypothesized that doxorubicin-dependent cardiotoxicity occurs through ROS production and possibly cellular iron accumulation. Here, we found that cardiotoxicity develops through the preferential accumulation of iron inside the mitochondria following doxorubicin treatment. In isolated cardiomyocytes, doxorubicin became concentrated in the mitochondria and increased both mitochondrial iron and cellular ROS levels. Overexpression of ABCB8, a mitochondrial protein that facilitates iron export, in vitro and in the hearts of transgenic mice decreased mitochondrial iron and cellular ROS and protected against doxorubicin-induced cardiomyopathy. Dexrazoxane, a drug that attenuates doxorubicin-induced cardiotoxicity, decreased mitochondrial iron levels and reversed doxorubicin-induced cardiac damage. Finally, hearts from patients with doxorubicin-induced cardiomyopathy had markedly higher mitochondrial iron levels than hearts from patients with other types of cardiomyopathies or normal cardiac function. These results suggest that the cardiotoxic effects of doxorubicin develop from mitochondrial iron accumulation and that reducing mitochondrial iron levels protects against doxorubicin-induced cardiomyopathy.

Introduction

Doxorubicin (DOX) is one of the most widely used antineoplastic drugs. The anticancer effects of DOX are believed to occur through the inhibition of topoisomerase enzyme and subsequent blockage of DNA resealing during cell replication (1). Despite its highly beneficial effects against cancer, the clinical use of DOX has the serious drawback of cardiotoxicity (2–4). The mechanism for DOX-induced cardiotoxicity is controversial, and several hypotheses have been proposed (4). It has been suggested that DOX induces an iron-mediated increase in ROS, referred to as the "ROS and iron hypothesis" (5, 6). According to this hypothesis, in the presence of iron, DOX leads to futile redox cycling, inducing substantial ROS production and cellular damage. Oxidation of the aglycone portion of DOX results in the formation of a semiquinone radical, which can rapidly revert to the parent compound by using O_2 as an electron acceptor (7). This redox cycle leads to the formation of superoxide, which is converted to H_2O_2 spontaneously or by superoxide dismutase. Subsequently, H_2O_2 may be converted to highly toxic hydroxyl radicals in the presence of heavy metals, such as iron, through the Fenton reaction. In addition, DOX can interact with iron directly to form a DOX-Fe complex, resulting in iron cycling between Fe(II) and Fe(III) forms and substantial ROS production (7–9).

The role of iron in DOX-induced cardiotoxicity has been supported by several studies. Systemic iron accumulation increases DOX-induced damage (10), and Hfe-deficient mice (a model of human hereditary hemochromatosis in which iron absorption from the intestinal tract is increased) have greater sensitivity to DOX (11). Furthermore, the iron chelator dexrazoxane (DXZ) has been demonstrated, in both preclinical and clinical studies, to reduce the cardiotoxic effects of DOX (12, 13). DXZ is currently the only FDA-approved drug for prevention of DOX-induced cardiotoxicity (13, 14). However, the "ROS and iron hypothesis" has been challenged, because numerous iron chelators, including some that are more potent and selective for iron than DXZ, have yielded negative or mixed results in preventing DOX-induced cardiotoxicity (4). The reason for the lack of uniformity among the effects of iron chelators on DOX-induced cardiotoxicity is unclear and has been the subject of several studies (15).

ABC protein-B8 (ABCB8, also referred to as mABC1) is a member of the ABC protein family. ABC transporters compose one of the largest families of proteins and are found in all species from bacteria to humans (16). We recently showed that ABCB8 has a role in mitochondrial iron homeostasis and cytosolic Fe/S protein maturation by facilitating mitochondrial iron export (17). Induced genetic deletion of ABCB8 in mouse hearts results in mitochondrial iron accumulation and development of cardiomyopathy, while its modulation in vitro causes changes in mitochondrial iron levels and export.

In this paper, we show that the cardiotoxicity of DOX occurs through preferential accumulation of iron specifically in the mitochondria and that a reversal in mitochondrial iron accumulation alleviates the deleterious effects of DOX on the heart. Treatment of cardiac cells with DOX increases mitochondrial iron levels, and overexpression of ABCB8 (which regulates mitochondrial iron export) reverses DOX-mediated toxicity both in vitro and in vivo. Furthermore, DXZ decreases mitochondrial iron content and cellular ROS in response to DOX and protects against DOX-induced cardiotoxicity, while deferoxamine (DFO), an effective iron chelator, does not reduce mitochondrial iron and does not exert cardioprotective effects.

Authorship note: Yoshihiko Ichikawa, Mohsen Ghanefar, Marina Bayeva, and Rongxue Wu contributed equally to this work.

Conflict of interest: Hossein Ardehali receives speaking honoraria from Merck and consulting honoraria from Cubist Pharmaceuticals. Yoshihiko Ichikawa is an employee of Novartis and receives income from the company.

Citation for this article: *J Clin Invest.* 2014;124(2):617–630. doi:10.1172/JCI72931.

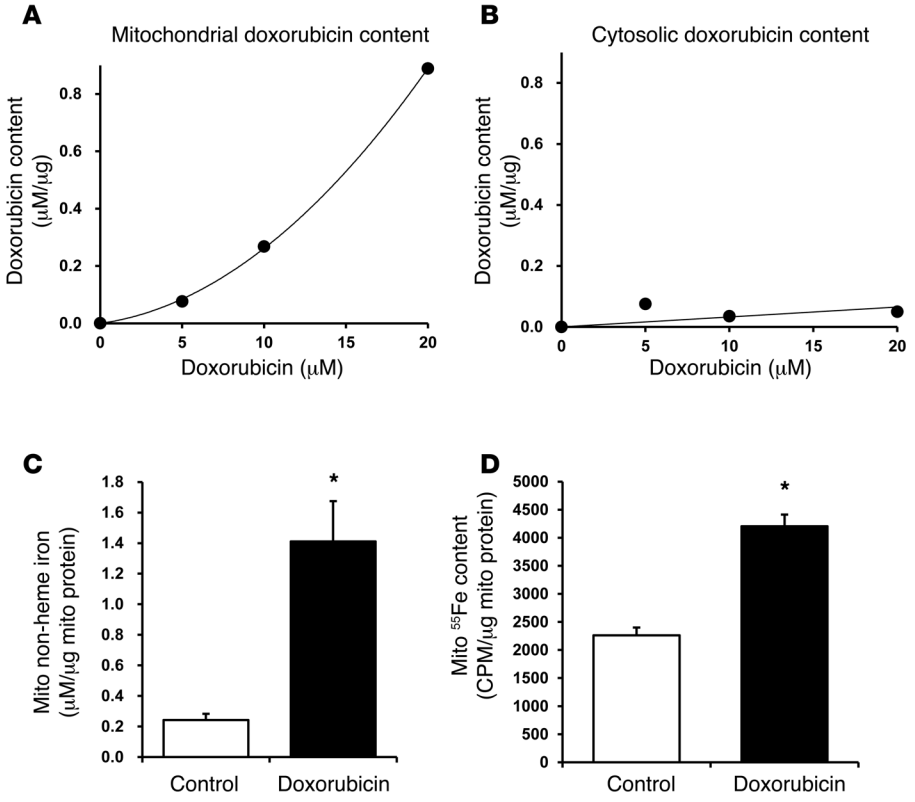

Figure 1
DOX regulates mitochondrial iron levels. DOX levels in the (**A**) mitochondrial and (**B**) cytosolic compartments of NRCMs after 16 hours of treatment with 10 μM DOX. (**C**) Mitochondrial iron levels, as assessed by colorimetric measurement of mitochondrial nonheme iron, in NRCMs that had been treated with DOX (10 μM) or a vehicle control for 16 hours (n = 5). (**D**) Mitochondrial iron levels, as assessed by measurement of ^{55}Fe, in DOX-treated NRCMs (10 μM for 16 hours, n = 4). Data are presented as mean ± SEM. *P < 0.05.

Results

DOX increases mitochondrial iron levels. DOX forms complexes with iron, and previous reports suggest that DOX concentrations may be higher in the mitochondria than in the cytoplasm (18, 19). We hypothesized that DOX accumulation in the mitochondria leads to increased mitochondrial iron levels. DOX exhibits prominent intrinsic absorbance (Supplemental Figure 1A; supplemental material available online with this article; doi:10.1172/JCI72931DS1), so this feature of DOX was used to measure its intracellular levels spectrophotometrically. Treatment of neonatal rat cardiomyocytes (NRCMs) with DOX resulted in a dose-dependent increase in mitochondrial DOX levels, while cytoplasmic levels of DOX remained low (Figure 1, A and B), suggesting that DOX accumulates in the mitochondria of cardiomyocytes. Treatment of NRCMs with 10 μM DOX for 16 hours also resulted in a significant increase in mitochondrial iron levels, as assessed by using the iron chelator bathophenanthrolinedisulfonate (BPS) (Figure 1C) and radiolabeled ^{55}Fe (Figure 1D). Moreover, oxygen consumption by the mitochondria and mitochondrial membrane potential were significantly reduced by DOX treatment (Supplemental Figure 1, B and C), indicative of mitochondrial dysfunction and consistent with previous reports (20, 21). These results suggest that DOX accumulates in the mitochondria and leads to an increase in mitochondrial iron levels.

To define the mechanism by which DOX increases mitochondrial iron, we assessed the effects of DOX on cellular and mitochondrial iron homeostasis. The total cellular iron levels were unaltered after DOX (Supplemental Figure 1D). DOX has previously been shown to inhibit the activity of iron regulatory protein 1 (IRP1) and IRP2 (22, 23), which bind to iron response elements (IREs) in 3′ or 5′ untranslated regions (UTRs) of target mRNA and result in their stabilization or degradation, respectively. Consistent with IRP1/2 inhibition, we observed a significant decrease in the expression of transferrin receptor 1 (TfR1) (Supplemental Figure 1E), a protein required for iron uptake into a cell and is positively regulated by IRP1/2 through the 4 experimentally validated IREs in its 3′UTR. Moreover, there was a concomitant increase in the levels of cellular iron exporter, ferroportin 1 (Supplemental Figure 1E), which is negatively regulated by IRP1/2 through its 5′UTR. To directly assess the activity of IRP1/2 in DOX-treated cells, we cloned either the full-length 3′UTR of TfR1 with all 5 IREs (TfR1-IRE) or the deletion construct with all 5 IREs removed (TfR1-IREΔ) upstream of luciferase reporter gene. Treatment of cells with DFO, an iron chelator that activates IRP1/2, significantly upregulated the expression of the full-length (Supplemental Figure 1F) but not the TfR1-IREΔ, construct (Supplemental Figure 1G). Having validated the specificity of our constructs, we assessed the effects of DOX on IRP1/2. Consistent with downregulation of *TFR1* mRNA, we observed suppression of full-length luciferase construct, while DOX treatment had no effect on the construct with IRE deletions (Supplemental Figure 1H). These results suggest that DOX regulates cellular iron through suppression of IRP1/2 function.

On a mitochondrial level, DOX significantly reduced the mRNA and protein levels of ABCB8 (a protein that regulates mitochondrial iron export) (Figure 2, A–E) and decreased or did not change levels of mitoferrin-2 (Mfrn-2, a regulator of mitochondrial iron import) (Figure 2, F and G) in vitro and in vivo. Moreover, consistent with increased mitochondrial iron, the mRNA and protein levels of iron storage protein mitochondrial ferritin were also increased (Figure 2H). These results suggest that the increase in mitochondrial iron is likely due to a decrease in iron export, and not an increase in import, from this organelle. Furthermore, the

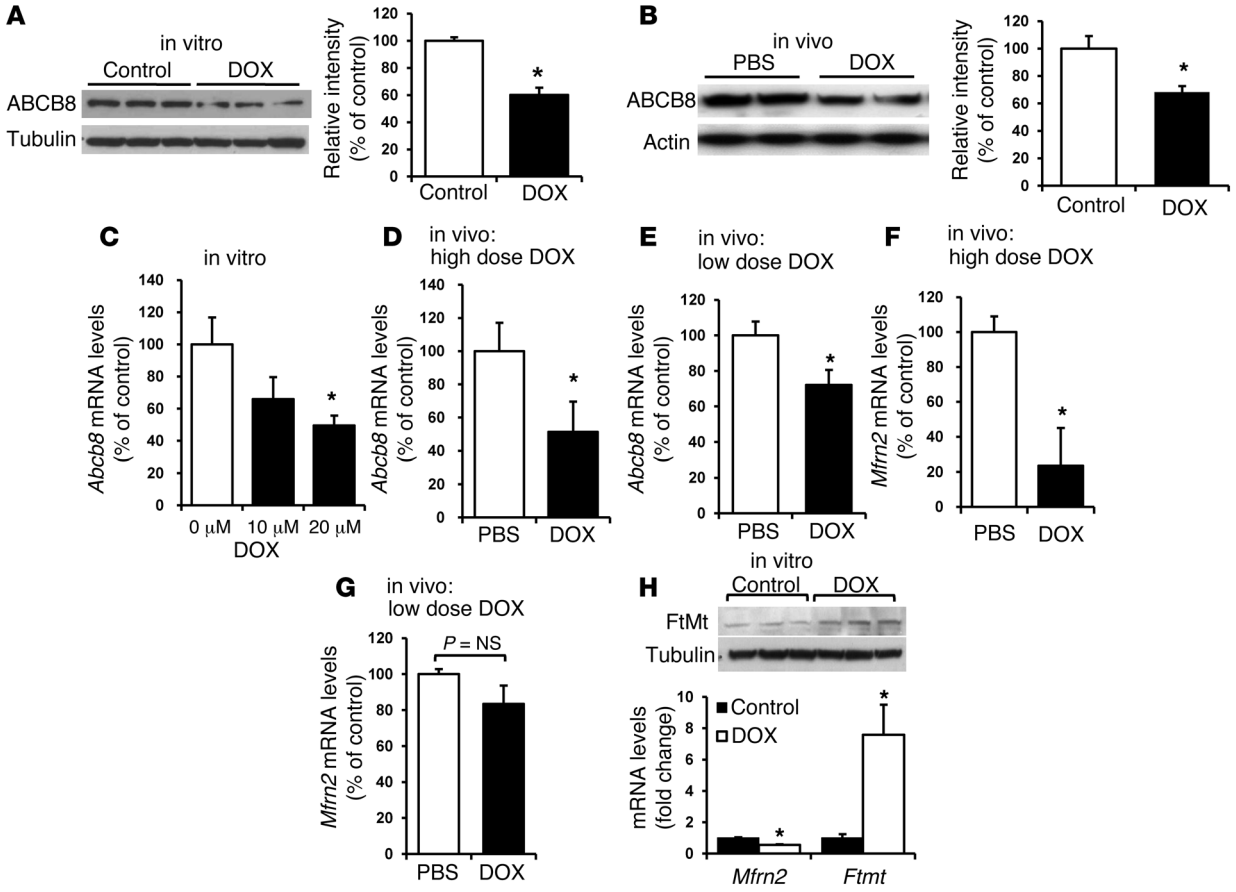

Figure 2

DOX regulates ABCB8 expression. (**A**) Western blot of ABCB8 in NRCMs after treatment with DOX (10 μM for 16 hours) or PBS. The results are summarized in the bar graph (n = 4). (**B**) Western blot of ABCB8 protein in mice after treatment with 4 intraperitoneal injections of 6 mg/kg/d DOX or PBS every third day. The hearts were harvested 1 month after completion of the protocol. The results are summarized in the bar graph (n = 6). (**C**) mRNA levels of *Abcb8* were measured in NRCMs treated with 0 μM, 10 μM, or 20 μM DOX (n = 4). (**D**–**G**) mRNA levels of (**D** and **E**) *Abcb8* (n = 5) and (**F** and **G**) *Mfrn2* (n = 4) were measured in the hearts of mice that had been treated with a high dose of DOX (10 mg/kg administered 3 times over 5 days) or a low dose of DOX (6 mg/kg every third day for 4 injections) or saline (PBS). (**H**) Western blot analysis of mitochondrial ferritin (FtMt) and *Mfrn2* and *Ftmt* mRNA levels in NRCMs treated with 10 μM DOX or control vehicle. Data are presented as mean ± SEM. *P < 0.05.

possible reduction in Mfrn-2 may be an adaptive response to halt the import of iron into the mitochondria. We next studied the mechanism by which DOX regulates ABCB8 levels. The effect of DOX on ABCB8 is likely direct, as the levels of other mitochondrial ABC proteins remained unchanged by DOX treatment both in vitro (Supplemental Figure 2A) and in vivo (Supplemental Figure 2B). However, to exclude the confounding effects of DOX on cell viability, we performed regulation experiments in HEK293 cells in which 10 μM DOX does not cause significant toxicity. In noncardiac HEK293 cells, treatment with a nontoxic dose of DOX (Supplemental Figure 2, C–E) led to a significant decrease in luciferase activity of a construct containing 6-kb ABCB8 promoter attached to a luciferase reporter (Supplemental Figure 2F). These results suggest that DOX regulates ABCB8 at the mRNA level and that this regulation is independent of cytotoxic effects of the drug.

ABCB8 modulation alters the cardiomyocyte response to DOX in vitro. To evaluate the role of ABCB8 in DOX-mediated mitochondrial iron accumulation and cellular damage, we modulated the levels of ABCB8 in NRCMs in the presence and absence of DOX and then assessed iron levels in various cellular compartments (mitochondria, nucleus, and cytosol), cellular ROS production, and cell viability. First, we showed that treatment of NRCMs with ABCB8 siRNA results in an effective reduction in the levels of the protein (Figure 3A) but no change in other mitochondrial ABC proteins (Supplemental Figure 3A). In the presence of DOX, ABCB8 siRNA resulted in a further increase in mitochondrial iron levels (Figure 3B) but had modest or no effect on iron levels in the nucleus or cytosol (Supplemental Figure 3, B–D). Importantly, nuclear and cytosolic iron levels were also similar between DOX- and vehicle-treated cells in the presence of ABCB8 downregulation (Supplemental Figure 3, C and D), suggesting that this drug preferentially increases iron content in the mitochondria. We next studied the effects of ABCB8 modulation and DOX on ROS production and cell death. While ABCB8 siRNA did not affect baseline cellular ROS levels, it resulted in a significantly higher ROS after DOX treatment (Figure 3, C and D). Furthermore, cell death, as assessed by MTS assay and TUNEL staining, was significantly higher after DOX treatment in response to ABCB8 silencing than in cells transfected with control siRNA (Figure 3, E and F). These results suggest that ABCB8 downregulation exacerbates the cytotoxic effects of DOX in vitro.

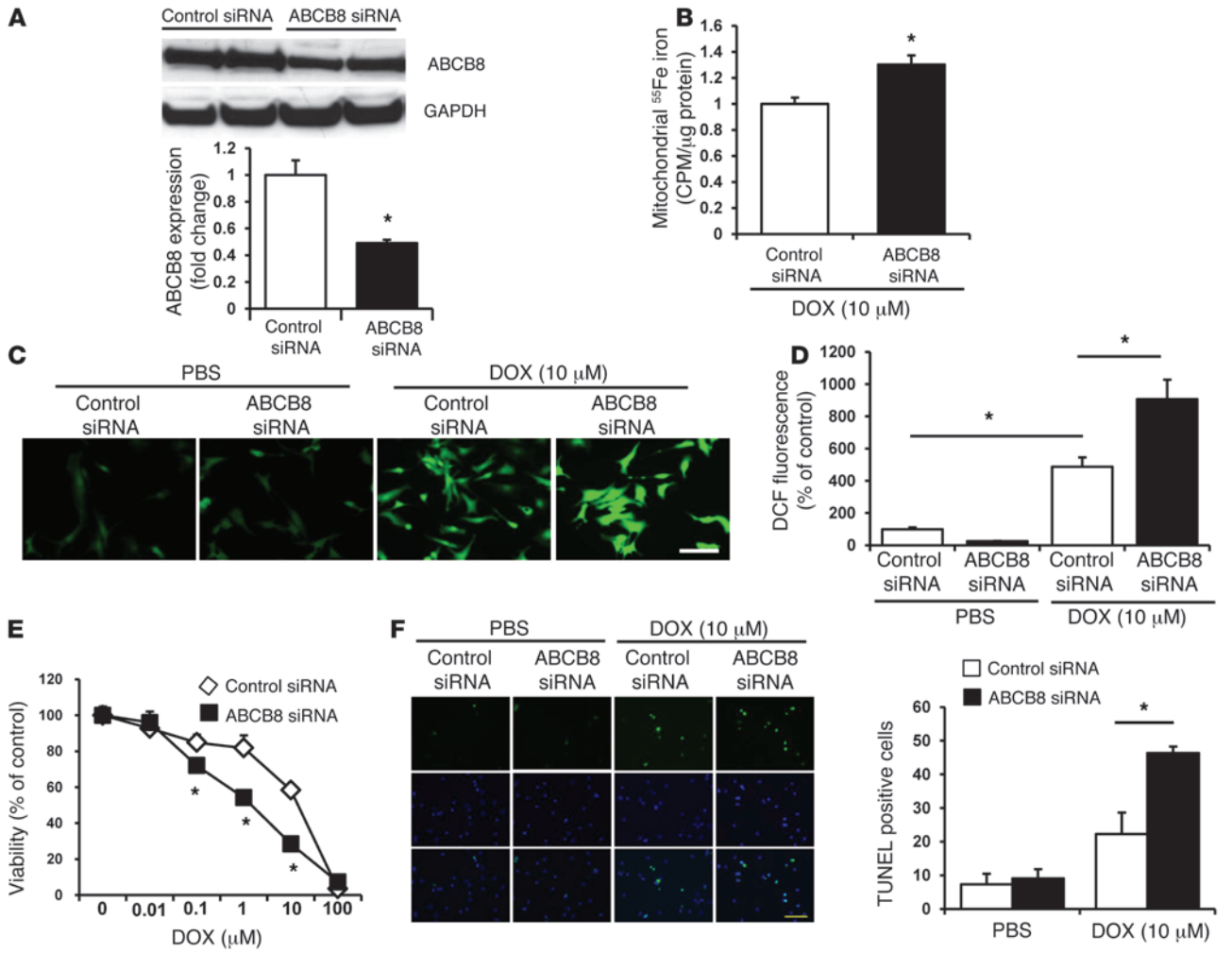

Figure 3

ABCB8 downregulation exacerbates the cardiotoxic effects of DOX in vitro. (**A**) Western blot of NRCMs treated with control and ABCB8 siRNA and probed with ABCB8 antibody, indicating effective reduction in ABCB8 protein levels with siRNA treatment ($n = 4$). (**B**) Mitochondrial iron levels, as assessed by measurement of ^{55}Fe, in cells transfected with control or ABCB8 siRNA and then treated with 10 μM DOX for 16 hours ($n = 4$). (**C**) Cellular ROS levels, as assessed by DCF, in NRCMs after treatment with 10 μM DOX for 16 hours. Scale bar: 100 μm. (**D**) Bar graph summary of the DCF studies ($n = 5$). (**E**) Cell viability, as assessed by MTS, in NRCMs transfected with control or ABCB8 siRNA and treated with increasing concentrations of DOX ($n = 6$). (**F**) DOX-induced cell death, as assessed by TUNEL staining, in cells transfected with control or ABCB8 siRNA. Quantification of the TUNEL staining is presented ($n = 3$). Scale bar: 100 μm. Data are presented as mean ± SEM. *$P < 0.05$ vs. control.

Next, we assessed whether ABCB8 overexpression can reverse the increase in mitochondrial iron levels and cell death observed in response to DOX treatment. ABCB8 overexpression reduced mitochondrial iron, as assessed by measurement of ^{55}Fe (Figure 4A), but not nuclear or cytosolic iron, which were also unchanged by DOX treatment (Supplemental Figure 4, A and B). We also measured the levels of chelatable mitochondrial iron by using the fluorescent probe rhodamine B 4-[(1,10-phenanthroline-5-yl) aminocarbonyl] benzyl ester (RPA), whose fluorescence diminishes with accumulating labile iron levels in the mitochondria (24, 25). The addition of DOX led to a reduction in RPA fluorescence in NRCMs that had been treated with a control GFP adenovirus, consistent with the accumulation of chelatable mitochondrial iron. This effect was attenuated by the overexpression of ABCB8 (Figure 4B), suggesting that ABCB8 overexpression reduces the DOX-induced accumulation of mitochondrial free iron. Compared to GFP, ABCB8 overexpression also reduced mitochondrial ROS levels (Figure 4, C and D) and cell death (Figure 4E) in the presence of DOX, suggesting that overexpression of ABCB8 is cytoprotective against DOX.

It may be argued that the protective effects of ABCB8 are due to the export of DOX from the mitochondria. To address this issue, we downregulated or overexpressed ABCB8 in NRCMs and then measured mitochondrial levels of DOX. As shown in Figure 4, F and G, DOX levels in the mitochondria did not change with ABCB8 downregulation or overexpression. These results suggest that the protective effects of ABCB8 result from changes in mitochondrial iron levels, rather than the export of DOX from the mitochondria.

ABCB8 transgenic mice are protected from DOX-induced cardiomyopathy. Our results suggest that the decline in mitochondrial iron levels caused by ABCB8 overexpression reduces the deleterious effects of DOX in cardiomyocytes in vitro. We extended our stud-

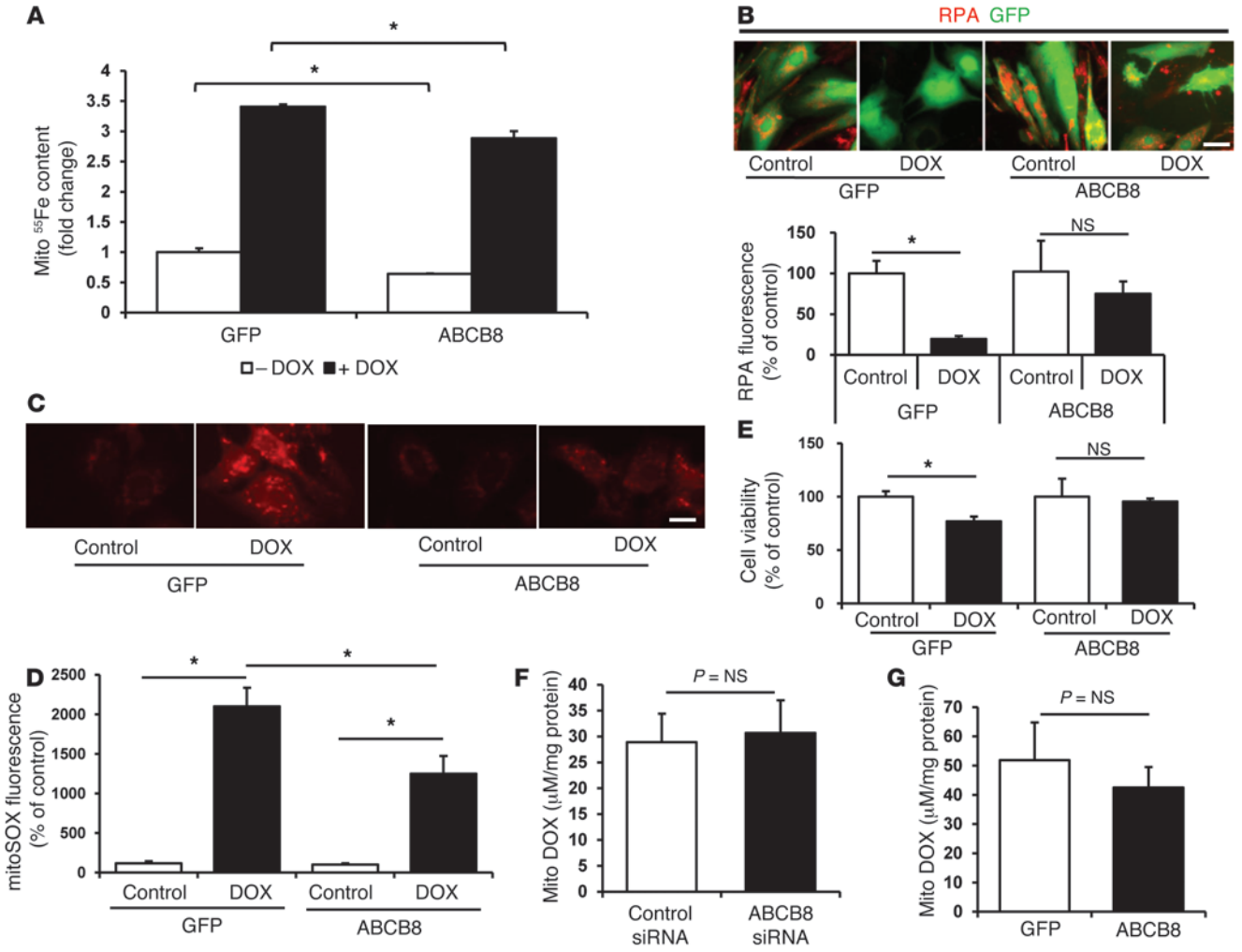

Figure 4

ABCB8 overexpression reduces DOX-induced mitochondrial iron accumulation and cardiotoxicity in vitro. (**A**) Mitochondrial iron levels, as assessed by ^{55}Fe in NRCMs transfected with adenoviruses coding for GFP or ABCB8 expression and treated with 10 μM DOX for 16 hours or vehicle control (n = 4). (**B**) RPA fluorescence in NRCMs transfected with the GFP or ABCB8 adenovirus and treated with 10 μM DOX for 16 hours. Lower levels of RPA fluorescence correspond to an increase in mitochondrial iron (n = 6). Scale bar: 100 μm. (**C**) ROS levels, as assessed by MitoSOX, in NRCMs transfected with the GFP or ABCB8 adenovirus and treated with DOX (10 μM for 16 hours) (n = 5). Scale bar: 100 μm. (**D**) Quantification of the ROS levels measured in **C**. (**E**) Cell viability, as assessed by MTS assay, in NRCMs transfected with the GFP or ABCB8 adenovirus and treated with 10 μM DOX for 16 hours (n = 6). (**F**) Mitochondrial DOX levels in NRCMs treated with control and ABCB8 siRNA, followed by treatment with 10 μM DOX for 16 hours (n = 4). (**G**) Mitochondrial DOX levels in NRCMs transfected with the GFP or ABCB8 adenovirus, followed by treatment with 10 μM DOX for 16 hours (n = 4). Data are presented as mean ± SEM. *P < 0.05.

ies to an in vivo model by generating transgenic (TG) mice that overexpressed ABCB8 in the heart (Figure 5A and Supplemental Figure 5, A and B). ABCB8 TG mice displayed significantly lower mitochondrial iron levels than those observed in non-TG (NTG) animals both at baseline and after treatment with DOX (Figure 5B), while no change in nuclear and cytosolic iron levels was observed (Supplemental Figure 5, C and D). Moreover, there was no change in mitochondrial iron levels in the lungs, livers, and kidneys of these mice (Supplemental Figure 5, E–G) as well as no alterations in hematologic iron parameters, including serum iron, unsaturated iron binding capacity, and total iron binding capacity (Supplemental Figure 5, H–J). At baseline, the TG mice had normal cardiac function and pressures and did not show any evidence of cardiomyopathy, as assessed by echocardiography, invasive hemodynamics, and histological analysis (Supplemental Figure 6, A–I). We subjected these animals to two different protocols of DOX treatment (Supplemental Figure 7A). Protocol 1 consisted of 10 mg/kg per day injections administered every other day for a total of 3 injections, and protocol 2 consisted of 6 mg/kg per day injections every third day for a total of 4 injections. Cardiac function was assessed 1 week after the last injection for protocol 1 and 1 month after the last injection for protocol 2; the earlier time point was chosen for protocol 1 due to early mortality of animals. Survival curves for TG and NTG animals after DOX treatment suggested marked mortality with protocol 1 (Supplemental Figure 7B) but not protocol 2 (Supplemental Figure 7C). Compared to NTG mice, TG mice subjected to DOX treatment according to protocol 2 had improved measurements of fractional shortening (FS), ejection

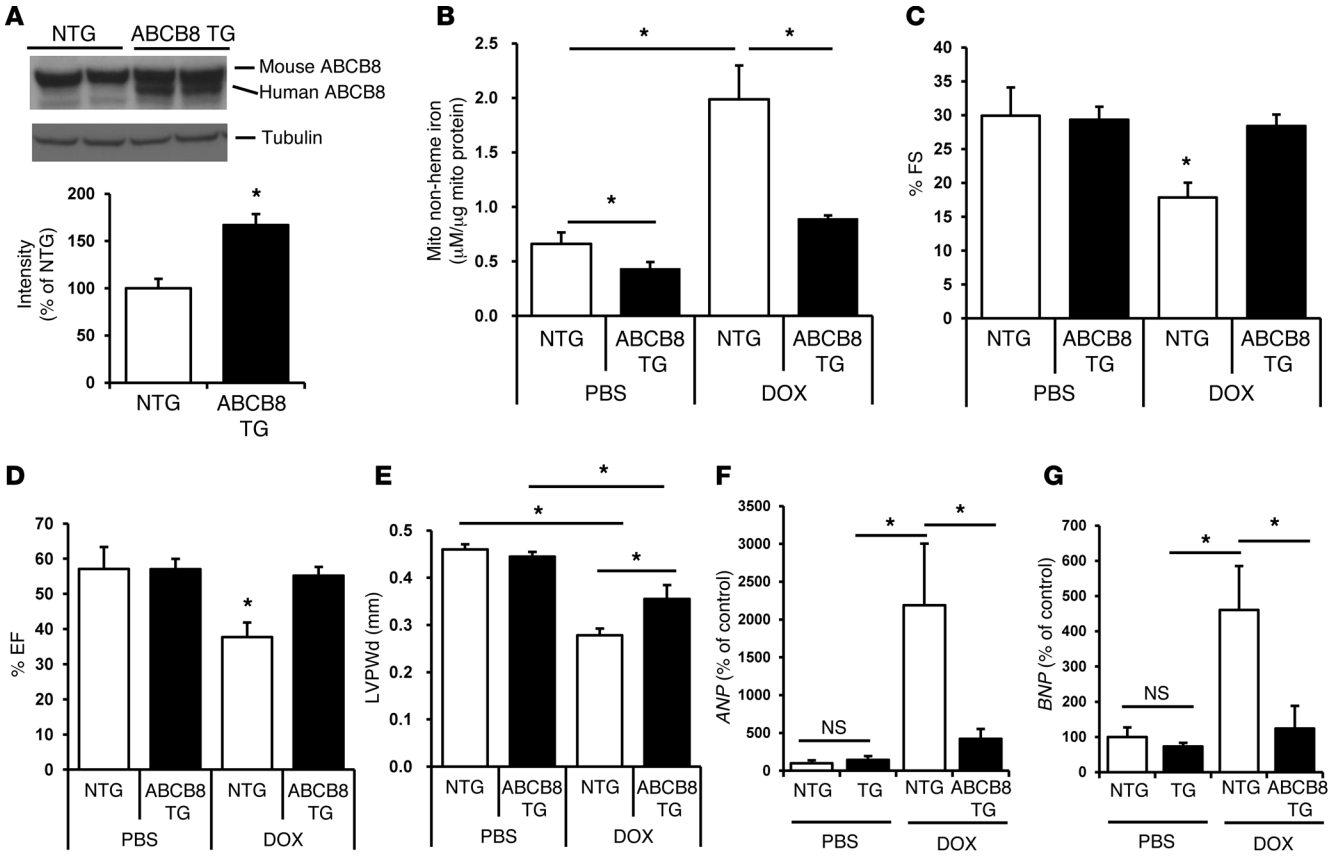

Figure 5

TG mice that overexpress ABCB8 in the heart are resistant to DOX cardiotoxicity. (**A**) Western blots demonstrating the overexpression of ABCB8 in the hearts of TG mice. Human ABCB8 migrates slightly lower than the mouse isoform. The results are summarized in the bar graph ($n = 4$). (**B**) Mitochondrial iron levels in NTG and ABCB8 TG mice at baseline ($n = 4$) and after treatment with DOX ($n = 5$) according to protocol 2. (**C**–**E**) Measurements of (**C**) FS, (**D**) EF, and (**E**) LVPWd in NTG and ABCB8 TG mice after DOX treatment according to protocol 2. ABCB8 TG mice maintained their cardiac systolic function after DOX treatment ($n = 4$–6 mice in each group). (**F** and **G**) Markers of heart failure, (**F**) *ANP* and (**G**) *BNP*, in NTG and ABCB8 TG mice ($n = 5$). Data are presented as mean ± SEM. $^*P < 0.05$.

fraction (EF), and increased left ventricular posterior wall thickness (LVPWd) after DOX treatment (Figure 5, C–E). Furthermore, the levels of atrial natriuretic peptide (ANP) and brain natriuretic peptide (BNP), markers for cardiomyopathy and heart failure, were significantly lower in TG mice compared with those in NTG mice after DOX treatment (Figure 5, F and G), while heart rate did not differ between the two groups (Supplemental Figure 7D). Similar protective effects were noted in ABCB8 TG animals that had been treated with protocol 1 (Supplemental Figure 7, E and F). Importantly, we observed no change in mitochondrial iron levels in livers, lungs, and kidneys after DOX treatment, and there was a slight increase in serum iron, with a corresponding decrease in unsaturated iron binding capacity in DOX-treated mice, while total iron binding capacity remained unchanged by DOX treatment (Supplemental Figure 5, H–J). Thus, overexpression of ABCB8 in the heart attenuates DOX-induced cardiomyopathy.

ABCB8 TG animals also displayed lower levels of lipid peroxidation products (a measure of oxidative stress) and reduced TUNEL positivity (a measure of cell death) than those observed in NTG mice after DOX treatment (Figure 6, A and B). Additionally, hearts from ABCB8 TG animals had preserved cardiomyocyte cross-sectional area (Figure 6C) and reduced perivascular fibrosis compared with hearts from NTG animals after treatment with DOX (Figure 6D). Electron microscopy examination revealed structural damage and mitochondrial deformities in NTG hearts after DOX treatment, while the structural integrity of mitochondria in TG animals was maintained, which corroborates the detrimental effects of DOX on mitochondria that were observed in vitro (Figure 6E). These results suggest that the overexpression of ABCB8 in the heart protects against DOX-induced cardiomyopathy by reducing mitochondrial iron levels and preserving mitochondrial structure.

Deletion of ABCB8 in the heart exacerbates DOX cardiotoxicity. We next assessed the effects of DOX on mice with cardiac-specific ABCB8 deletion (cs-*Abcb8*$^{-/-}$ mice). Mice with LoxP sequences flanking exon 1 of ABCB8 were crossed with mice that express Cre surrounded by mutant estrogen receptor and under α-MHC promoter (α-MHC-MCM mice) (17). Deletion of the gene occurs after the mice are treated with oral tamoxifen, as described previously (17). These mice develop spontaneous cardiomyopathy and an increase in mitochondrial iron levels, and their phenotype has been previously reported (17). Treatment of cs-*Abcb8*$^{-/-}$ mice with DOX resulted in a significant deterioration of cardiac function parameters, including FS and EF compared with the wild-type littermate control mice treated with tamoxifen and DOX (Figure 7, A–C). Fur-

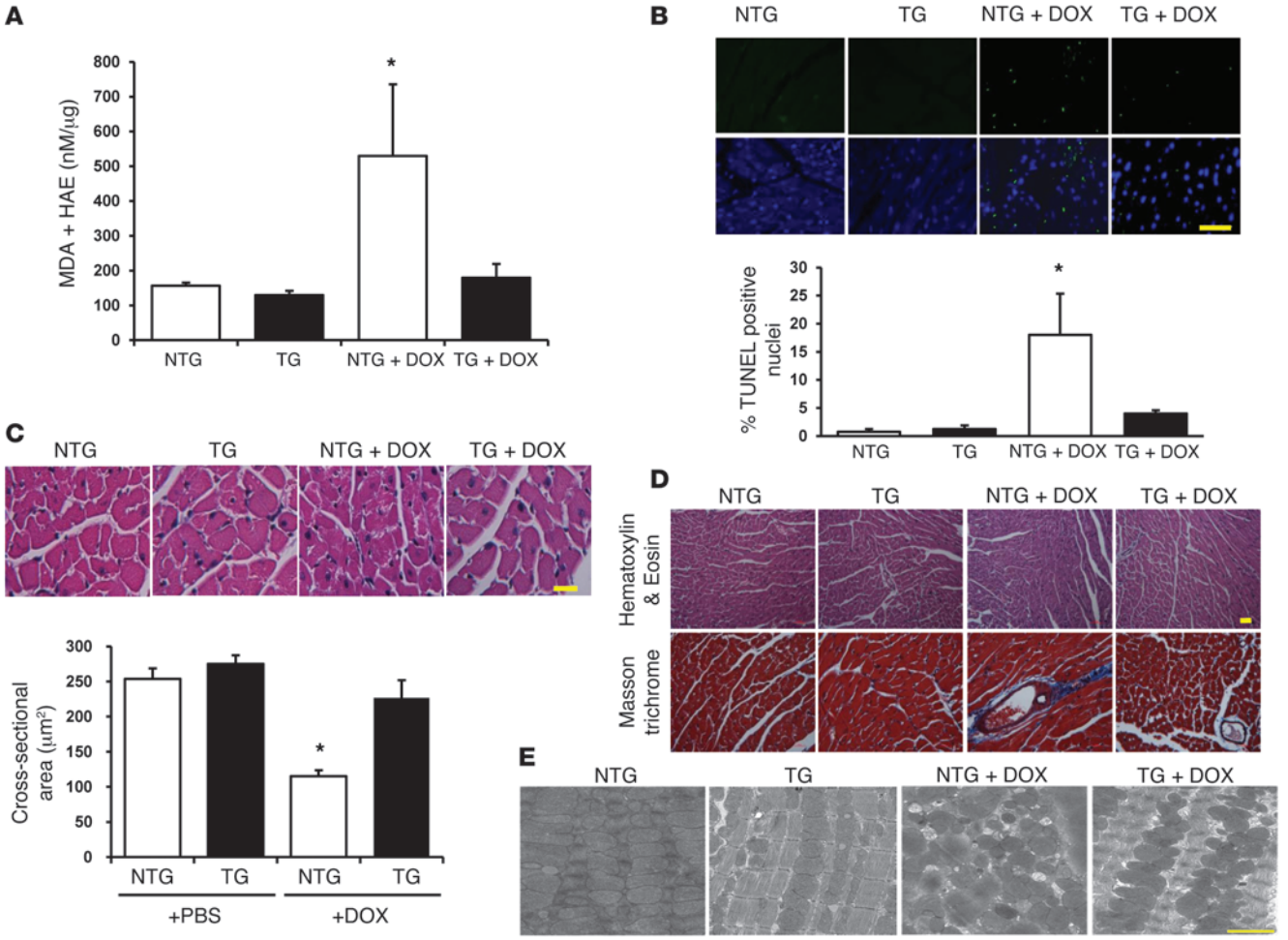

Figure 6

Hearts from ABCB8 TG mice display reductions in ROS and structural damage in response to DOX. (**A**) Lipid peroxidation products (i.e., markers of cellular ROS levels) in ABCB8 TG and NTG hearts in the presence and absence of DOX treatment, as assessed by measurement of MDA and HAE (n = 6). (**B**) TUNEL-positive cells in NTG and ABCB8 TG hearts in the presence and absence of DOX treatment (n = 3). Scale bar: 200 μm. (**C**) H&E staining for assessment of cardiomyocyte size in NTG and TG hearts at baseline and after treatment with DOX. A summary of cardiomyocyte size in the H&E-stained sections (n = 4) is shown. Scale bar: 200 μm. (**D**) Assessment of fibrosis by Masson trichrome staining of ABCB8 TG and NTG hearts after DOX treatment. Scale bar: 100 μm. (**E**) Representative electron microscopy images of hearts from NTG and ABCB8 TG mice after treatment with PBS or DOX. Hearts from the ABCB8 TG mouse treated with DOX show well-aligned mitochondria, with clearly distinguishable cristae. Scale bar: 1 μm. Data are presented as mean ± SEM. *P < 0.05.

thermore, DOX resulted in a significant increase in left ventricular diastolic diameter (LVDd) in cs-*Abcb8*$^{-/-}$ mice but not in wild-type animals (Figure 7D). These results suggest that mice with ABCB8 deletion in the heart and the resultant increase in mitochondrial iron are more susceptible to the cardiotoxic effects of DOX, as evidenced by worsened cardiac function.

DXZ reverses DOX-induced mitochondrial iron accumulation. DXZ is an iron chelator that is FDA-approved for the prevention of DOX-induced cardiomyopathy (12). However, more potent and specific iron chelators, such as DFO, have failed to provide similar protective effects (26). We hypothesized that the protective effects of DXZ occur through the selective reduction of mitochondrial iron levels and that DFO is ineffective because it fails to target and reduce mitochondrial iron. Thus, we compared the efficacy of DXZ and DFO at lowering mitochondrial iron levels in the presence of DOX. While DXZ reduced mitochondrial iron levels in NRCMs after DOX treatment, the effect of DFO was minimal, as determined by the BPS (Figure 8A) and RPA (Figure 8B) assays. Failure of DFO to chelate mitochondrial iron is consistent with the poor mitochondrial permeability of the drug (27, 28). Importantly, DXZ had no effect on the levels of nuclear and cytosolic iron in control NRCMs and led to only slight reduction in nuclear iron in DOX-treated cells, consistent with its low potency in chelating iron, while DFO reduced iron levels in both of these cellular compartments by 50% in the presence and absence of DOX (Supplemental Figure 8, A and B). To further rule out the lack of cell penetrance of DFO or its inactivity under our experimental conditions, we measured the effects of DFO on TfR1, whose induction is a well-described response to iron chelation. Treatment of NRCMs with DFO resulted in a significant increase in the mRNA levels of *TFR1* (Figure 8C), indicating that DFO penetrated the cells and was biologically active under our experimental conditions.

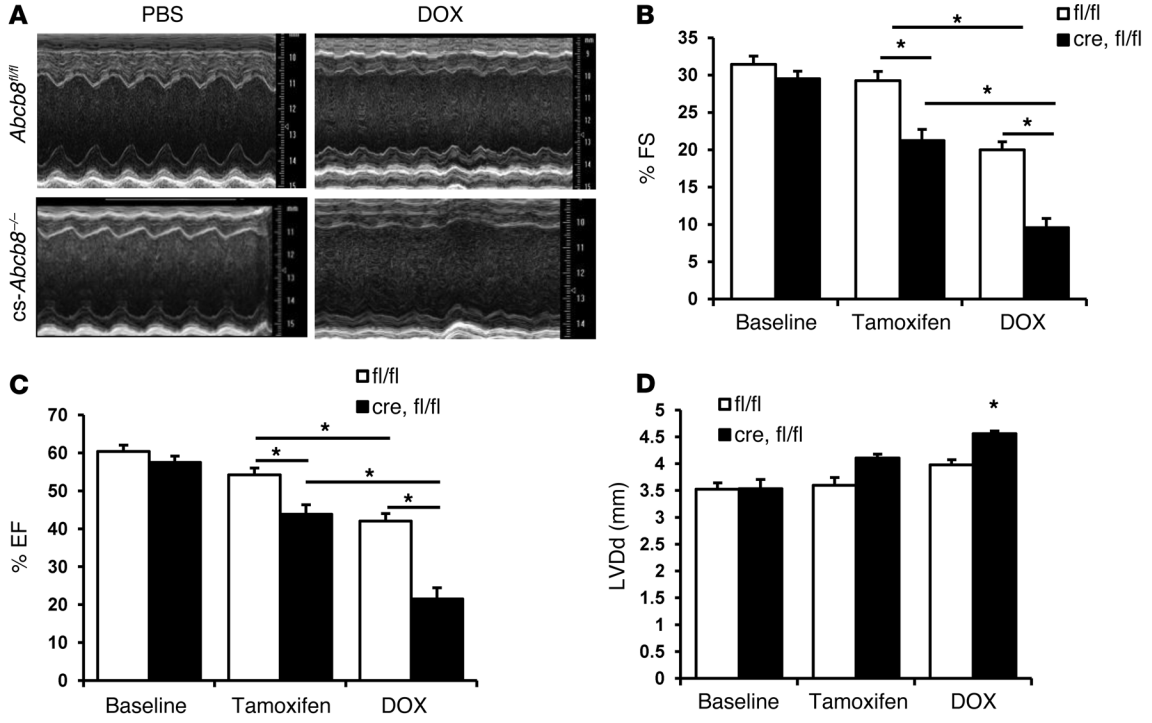

Figure 7
Treatment of mice with ABCB8 deletion in the heart leads to exacerbated cardiomyopathy. (**A**) Echocardiography images of control (*Abcb8*$^{fl/fl}$) and *Abcb8*$^{fl/fl}$ mice crossed with α-MHC-MCM mice (i.e., cs-*Abcb8*$^{–/–}$ mice) after treatment with PBS or DOX and treatment with tamoxifen. (**B**) FS, (**C**) EF, and (**D**) LVDd in *Abcb8*$^{fl/fl}$ mice or *Abcb8*$^{fl/fl}$ mice (fl/fl) crossed with α-MHC-MCM animals (cre,fl/fl) at baseline after treatment with tamoxifen and after treatment with tamoxifen and DOX (n = 4–5). Data are presented as mean ± SEM. *P < 0.05.

We next studied the effects of DFO and DXZ on mitochondrial iron and cardiac function in mice after treatment with DOX. Consistent with our in vitro studies, levels of mitochondrial iron were similar in the hearts of control mice treated with DOX alone and in the hearts of mice treated with DFO and DOX (3.11 ± 0.16 μM iron/μg mitochondrial protein for DOX alone vs. 3.11 ± 0.14 μM iron/μg mitochondrial protein for DOX and DFO, n = 4, P = 0.98); however, treatment of mice with DOX and DXZ significantly reduced mitochondrial iron levels (2.75 ± 0.03 μM iron/μg mitochondrial protein, n = 4, P = 0.037 vs. DOX alone, P = 0.004 vs. DOX and DFO), as measured by Ferene S-based assay. No difference was observed in cytosolic and nuclear iron levels between the treatment groups (Supplemental Figure 8, C and D). Improvements in FS (a measure of cardiac function) were significantly greater in mice treated with DXZ than in mice treated with DFO (Figure 8D). DOX has also been shown to cause thinning of cardiac walls, and a recent study suggests that DXZ reverses this detrimental effect of DOX in children with acute lymphoblastic leukemia (29). Consistent with these observations, we noted that DXZ reversed the effect of DOX on LVPWd, while DFO had no effect (Figure 8E). Furthermore, DXZ, but not DFO, was associated with significantly lower mRNA levels of *ANP* and *BNP*, markers of cardiac dysfunction, after DOX treatment (Figure 8, F and G). None of the treatments altered heart rate (Supplemental Figure 8E). These results indicate that DXZ, but not DFO, preferentially lowers mitochondrial iron levels and significantly decreases the cardiotoxic effects of DOX, which supports the hypothesis that the protective effects of DXZ and the ineffectiveness of DFO result from their differing abilities to reduce mitochondrial iron levels.

Mitochondrial iron regulates toxicity of DOX independent of topoisomerase-2β pathway. Recently, Zhang et al. reported that mice with deletion of topoisomerase-2β (Top-2β) in the heart are protected from DOX cardiotoxicity, arguing that Top-2β mediates the damaging effects of DOX on the heart (30). Moreover, DXZ was previously shown to inhibit Top-2β (31, 32), suggesting that, in addition to reducing mitochondrial iron, DXZ may protect the heart through Top-2β suppression. To determine whether there is interplay between mitochondrial iron and Top-2β pathways in mediating DOX toxicity, we first asked whether Top-2β is involved in mitochondrial iron regulation by DOX. We used an siRNA approach to knock down the expression of Top-2β in NRCMs in the presence of DOX (Figure 9A) but found no difference in mitochondrial or cytosolic iron levels in these cells (Figure 9, B and C). Moreover, Top-2β siRNA had no effect on the expression of ABCB8 protein in DOX-treated NRCMs (Figure 9A). These data suggest that Top-2β does not regulate mitochondrial iron levels.

Next, we asked whether mitochondrial iron can regulate Top-2β expression, i.e., whether Top-2β functions downstream of mitochondrial iron in DOX cardiotoxicity. Pharmacologic reduction in mitochondrial iron using DXZ reduced Top-2β, consistent with previous reports (31, 33, 34), while DFO had no effect on Top-2β protein (Figure 9D). However, genetic reduction in mitochondrial iron through adenoviral overexpression of ABCB8 in NRCMs (Figure 9E) or TG expression of ABCB8 in mouse hearts (Figure 9F) did not alter Top-2β protein, arguing that Top-2β function in DOX toxicity is independent of that of mitochondrial iron accumulation. Thus, we conclude that reduc-

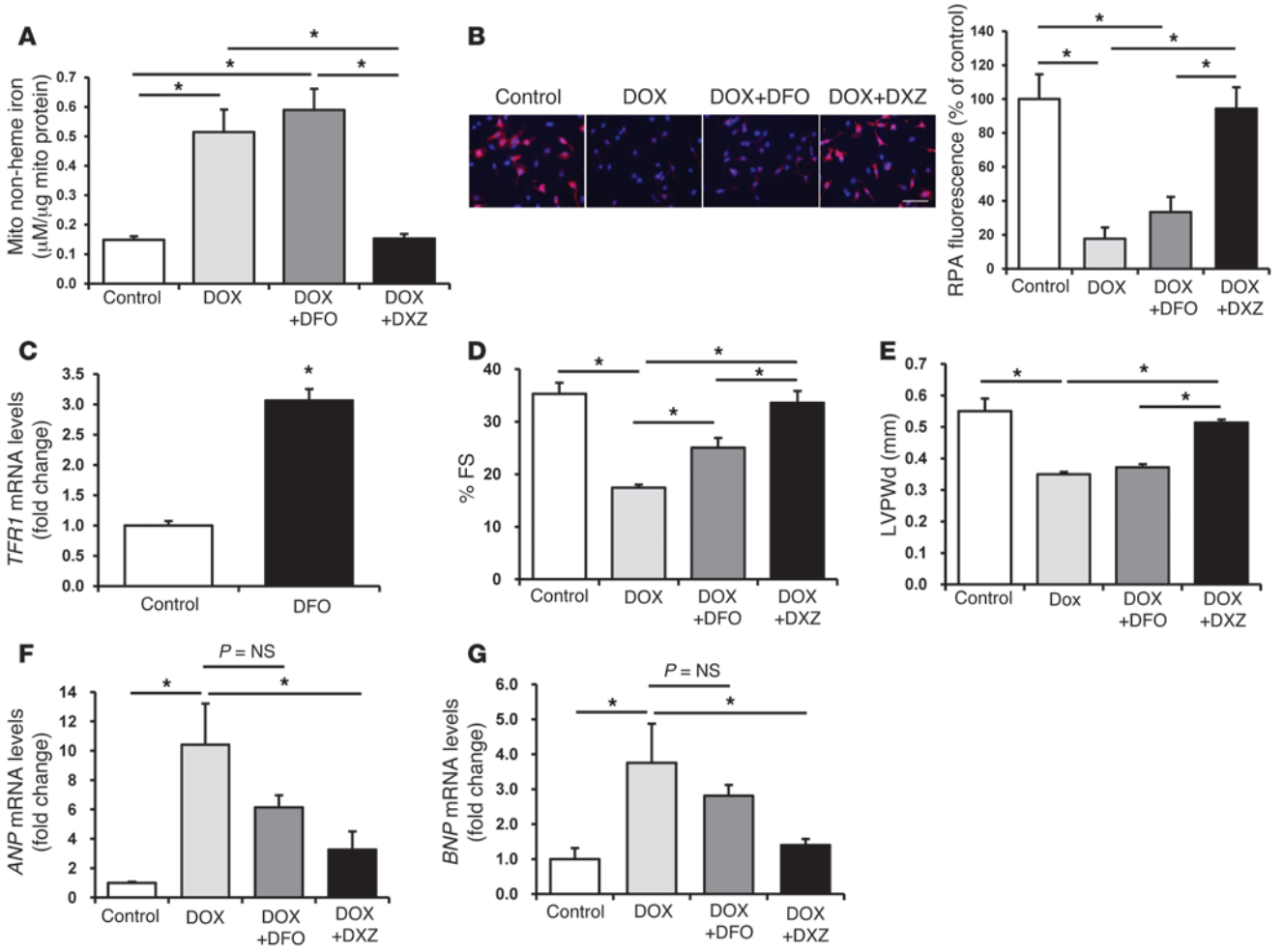

Figure 8

DXZ reduces mitochondrial iron and reverses the cardiotoxic effects of DOX. (**A**) Mitochondrial nonheme iron levels in NRCMs, as assessed by BPS after treatment with or without DXZ (100 μM) or DFO (200 μM) in the presence of 10 μM DOX for 16 hours ($n = 4$). (**B**) Levels of mitochondrial iron in NRCMs, as assessed by RPA staining after treatment with or without DXZ (100 μM) or DFO (200 μM) in the presence of 10 μM DOX for 16 hours ($n = 4$). Scale bar: 100 μm. A summary of the RPA data is shown. (**C**) Levels of *TFR1* mRNA in NRCMs at baseline (control) and after treatment with DFO (200 μM, $n = 6$). (**D**) FS and (**E**) LVPWd in control and DOX-treated mice that had been cotreated with or without DXZ or DFO ($n = 6$). (**F** and **G**) Levels of (**F**) *ANP* and (**G**) *BNP* in the hearts of mice treated with DOX, DOX, and DFO or DOX and DXZ ($n = 4$). Data are presented as mean ± SEM. *$P < 0.05$.

tion in mitochondrial iron and Top-2β deletion exert cardioprotection through independent mechanisms.

Mitochondrial iron levels are increased in the hearts of patients with DOX-induced cardiomyopathy. Finally, we assessed the effects of DOX on mitochondrial iron levels in patients with DOX-induced cardiomyopathy. Explanted hearts from patients who underwent cardiac transplant due to DOX toxicity, hearts from patients with cardiomyopathy from other causes, and hearts from patients with normal cardiac function were used for these studies. Mitochondrial nonheme iron levels were found to be significantly higher in the hearts of patients with DOX-induced cardiomyopathy, compared with those in controls, including normal hearts and hearts with cardiomyopathy due to other causes (Figure 9G). Furthermore, cytosolic iron levels were lower (but not statistically significant) in DOX-treated patients (Figure 9H). Although studies on explanted human heart samples have intrinsic limitations (including lack of knowledge of duration of therapy, dosage of DOX, the demographics of subjects, a time lag between DOX treatment and heart transplant, and possible damage to the mitochondrial structure during tissue isolation and storage), these results support our findings that DOX-induced cardiomyopathy is associated with an increase in mitochondrial iron.

Discussion

The mechanisms of DOX-induced cardiotoxicity have been studied extensively but remain controversial. Myocardial oxidative damage due to iron-mediated ROS formation has been suggested as a potential mechanism, but the "ROS and iron hypothesis" has been challenged by reports that several iron chelators fail to reverse the cardiotoxic effects of DOX (4). Our data suggest that DOX cardiotoxicity develops from the specific accumulation of iron in the mitochondria and that DXZ, which can effectively

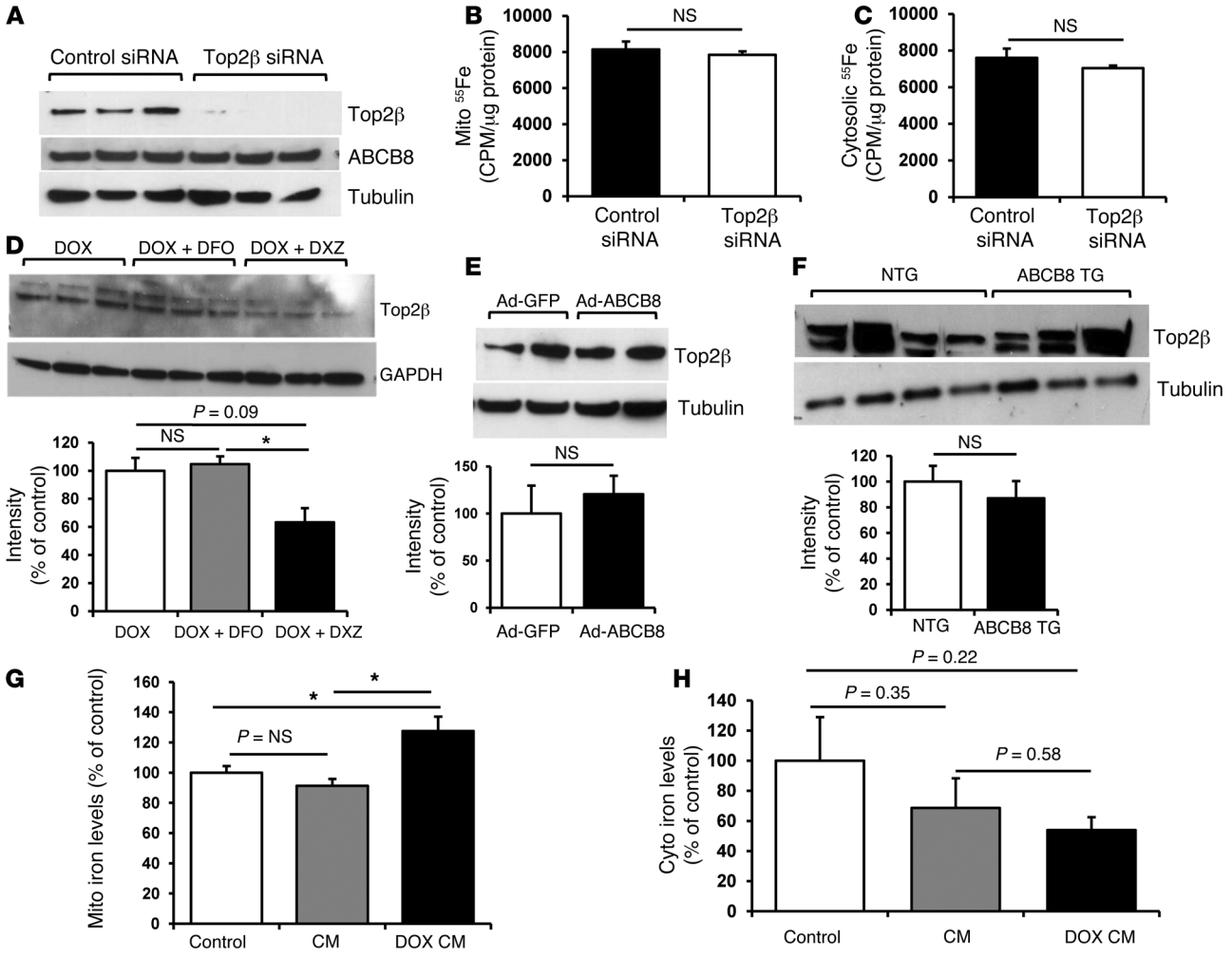

Figure 9

Cytotoxicity of DOX through mitochondrial iron is independent of the Top-2β pathway. (**A**) Western blot analysis of Top-2β and ABCB8 expression in NRCMs treated with Top-2β or control siRNA, showing efficient reduction in Top-2β protein with siRNA treatment but no change in ABCB8 protein level. (**B**) Mitochondrial and (**C**) cytosolic iron levels determined by quantification of ^{55}Fe radioactivity in NRCMs with Top-2β or control siRNA (n = 4). (**D**–**F**) Western blot analysis of Top-2β protein (**D**) in NRCMs treated with 10 μM DOX with or without 200 μM DXZ or 200 μM DFO for 16 hours, (**E**) in NRCMs with adenoviral overexpression of ABCB8, or (**F**) in ABCB8 TG and NTG mice treated with DOX. (**G**) Mitochondrial iron and (**H**) cytosolic iron levels in heart samples from patients without cardiomyopathy (control), patients with cardiomyopathy from non–DOX-related causes (CM), or patients with DOX-induced cardiomyopathy (DOX CM) (n = 5). Data are presented as mean ± SEM. *P < 0.05.

reverse the cardiotoxic effects of DOX, works by reducing mitochondrial iron levels.

Although several studies have supported the role of iron in DOX-induced cardiotoxicity (10–13), this hypothesis has been challenged by the lack of efficacy of several iron chelators that are more potent and selective for iron than DXZ. DFO, a highly effective iron chelator that has been used historically to treat cardiac iron overload in patients with thalassemia (35), has been shown to exert protective effects in vitro only in Fe-overloaded cells (36, 37), while studies in animal models and human patients have yielded conflicting results (26). In our studies, DFO was efficiently taken up by the cells (based on the upregulation of TfR1, a well-established target that is increased during iron chelation); however, it failed to reduce mitochondrial iron levels, perhaps because its accessibility to iron pools contained inside membrane-bound organelles is limited (38). Two other orally effective iron chelators, deferiprone and deferasirox, also fail to protect against DOX-induced cardiac damage (39, 40), and aroylhydrazone Fe chelators (e.g., pyridoxal isonicotinoyl hydrazone and its analogs), which are small lipophilic molecules, provide less protection than DXZ against DOX toxicity as well (4). This discrepancy in the effects of different iron chelators could be due to their varying effectiveness in reducing mitochondrial iron, which we demonstrate here for DFO and DXZ. Finally, it should be noted that, in addition to removing iron from the mitochondria, iron chelators also physically sequester iron and make it unavailable for cellular processes. Thus, the degree of reduction in the physiologically available iron (vs. total iron) may be significantly more pronounced with DXZ than that detected in our assay. Nevertheless, our findings strongly suggest the need for development of novel iron chelators that can effectively and preferentially reduce mitochondrial iron.

We also studied the mechanism by which DOX leads to preferential accumulation of iron in the mitochondria. Our data demonstrated that DOX downregulates ABCB8, which is consistent with impaired iron export from the mitochondria, while Mfrn-2 levels are not changed or decreased, possibly as a compensatory response to the increased mitochondrial iron levels. It is also possible that DOX may interact with and "capture" iron within the mitochondria; however, our data showed that modulation of ABCB8 did not alter mitochondrial DOX levels, making this possibility less plausible. In addition to altering mitochondrial iron, DOX was shown to directly regulate cellular iron homeostasis through several mechanisms. First, DOX was found to suppress RNA-binding activity of both IRPs through posttranscriptional modifications and interactions with the [4Fe/4S] cluster in IRP1 (22, 23). In addition, DOX was shown to alter iron trafficking inside the cell by increasing iron incorporation into ferritin and suppressing iron release from cellular stores (41, 42). Thus, although DOX is predicted to reduce cellular iron import via suppression of IRPs, normal cytosolic iron levels are likely maintained through reduced turnover of ferritin and decrease in iron release from cytoplasmic stores. Overall, the effects of DOX on cellular iron regulation are very different from all other models of mitochondrial iron accumulation and may indirectly influence iron metabolism inside the mitochondria.

A recent study has identified Top-2β as another molecular mediator of DOX cardiotoxicity through activation of DNA damage response pathway and induction of apoptosis (30). Iron and topoisomerases are two well-known targets of DOX. Inhibition of topoisomerase is the main mechanism for the antineoplastic effects of DOX, while iron is thought to enhance ROS generation in the presence of DOX (4). Our results, along with those of Zhang et al. (30), suggest that targeting both mitochondrial iron and topoisomerases is protective against cardiotoxicity of DOX. However, it remains unclear how Top-2β and mitochondrial iron pathways relate to each other in their modulation of DOX-induced cardiac damage. There may be a yet unidentified link between mitochondrial iron homeostasis and topoisomerases, as several iron chelators, including DXZ, were also shown to inhibit Top-2α/2β activities (43). However, the protective effects reported here are likely independent of the topoisomerase pathway, since a topoisomerase-inactive analog of DXZ that retains its iron-chelating properties confers a similar degree of protection to its parent compound (44), and also genetic overexpression of ABCB8 confers protection comparable to that of DXZ. Moreover, we show that reduction in mitochondrial iron levels through overexpression of ABCB8 in vitro and in vivo does not alter Top-2β protein levels and knockdown of Top-2β has no effect on ABCB8 protein expression or mitochondrial iron content in NRCMs. Thus, the two pathways are likely to mediate the effects of DOX on the heart independent of each other. Although both studies reported significant and almost complete protection against DOX toxicity, our study design and protocol of DOX administration differ from those of Zhang et al., and thus we were unable to directly compare relative contributions of mitochondrial iron and Top-2β deletion to cardioprotection. Studying the two pathways separately and in combination to assess their additive effects on the heart and to guide the development of clinical therapies targeting these pathways is warranted.

Although DXZ has been approved by the FDA for treatment of DOX-induced cardiomyopathy, this compound is rarely used in clinic due to its multiple side effects and concerns about reducing the antineoplastic efficacy of DOX through inhibition of Top-2α (45). Moreover, DXZ treatment is linked to the development of hematologic malignancies, particularly acute myeloid leukemia and myelodysplastic syndrome (46, 47). Based on these studies, European Medicines Agency now recommends against the use of DXZ with DOX treatment (48). Despite significant toxicities associated with DXZ use, consideration of underlying principles behind its cardioprotective action is critical for the development of novel treatments for DOX toxicity. Thus, the Top-2β–inactive analog of DXZ, which retains its iron-chelating properties and does not induce myelosuppression, was shown to exhibit a similar degree of protection against DOX (44). This finding, together with our data on DXZ efficacy in chelating mitochondrial iron, provides an important foundation for the development of drugs that can access the mitochondrial iron pool, without side effects associated with DXZ use.

Finally, we would like to acknowledge that our study has several limitations. First, mitochondrial iron accumulation likely represents one of several mechanisms of DOX cardiotoxicity, some of which may not have been identified yet, and the relationship between mitochondrial iron and other pathways of DOX cardiotoxicity is not known. Furthermore, the mechanism by which DOX accumulates in the mitochondria of cardiomyocytes is not entirely clear. We provide evidence that DOX suppresses expression of ABCB8 protein, functioning in iron transport out of the mitochondria; however, other mechanisms, such as iron capturing by DOX and effects of DOX on IRP1/2 proteins, may also contribute. Finally, we have not shown that reduction in mitochondrial iron is protective against DOX toxicity in humans, although our data in several different animal models and the fact that mitochondrial iron levels are increased in human hearts with DOX-induced heart failure suggest that the same mechanism may be operational in human patients.

In summary, our results demonstrate that reducing mitochondrial iron levels effectively reverses DOX-induced cardiomyopathy. We show that DOX increases mitochondrial iron levels and that overexpression of the mitochondrial iron export modulator ABCB8 or treatment with DXZ reduces mitochondrial iron levels and cardiac damage from DOX both in vitro and in vivo. Furthermore, hearts from patients with DOX-induced cardiomyopathy displayed increased mitochondrial iron levels. These results suggest two potential approaches for reversing DOX-induced cardiomyopathy: the identification of novel iron chelators that effectively and preferentially reduce mitochondrial iron in the heart and the development of pharmacological agents that increase the rate of mitochondrial iron export, perhaps by upregulating ABCB8 expression.

Methods

DOX treatment of the cells. Cells were treated for 16 hours with various concentrations of DOX hydrochloride (Sigma-Aldrich) in complete growth medium.

Measurement of iron. The total mitochondrial nonheme iron was measured by spectrophotometry using the iron chelator BPS (Sigma-Aldrich) (49). Isolated mitochondria (0.1–1 mg) were suspended in 1 ml of 10 mM 2-(N-morpholino) ethanesulfonic acid or MES (pH 4.5) and 1% (w/v) sodium dodecyl sulfate. BPS, to a final concentration of 50 μM, and 1 μl of a saturated dithionate stock solution were added to the mixture. The formation of the Fe(II)-BPS complex was determined from the difference between the absorption at 540 nm and 575 nm, using ferric citrate (Sigma-Aldrich) to generate a standard curve. For determination of

mitochondrial ^{55}Fe content, NRCMs were grown in the presence of 150 to 250 nM NTA-conjugated ^{55}Fe for 48 hours. Mitochondrial isolation was performed using the Mitochondria Isolation Kit for Cultured Cells (Thermo Scientific) according to the manufacturer's protocol, with an additional wash of mitochondrial pellet with cold 500 μM BPS in PBS to remove membrane-associated radioactivity. Mitochondrial ^{55}Fe content was analyzed on a Beckman liquid scintillation counter and normalized to mitochondrial protein content. Finally, mitochondrial iron was determined using the Ferene S-based Iron Assay Kit (BioVision) according to the manufacturer's protocol. Briefly, iron was released from carrying proteins in the presence of acidic buffer, followed by reduction into ferrous form and reaction with Ferene S to produce a stable blue-colored product. The absorbance was quantified spectrophotometrically at 593 nm and normalized to the protein concentration of each sample. Mitochondrial ferritin antibody was a gift from Paolo Arosio (Università di Brescia, Brescia, Italy).

Mitochondrial Fe^{2+} detection. Detection of free mitochondrial iron was performed using RPA (Squarix Biotechnology GmbH). NRCMs were treated with 10 μM DOX for 16 hours. Cell culture media was then removed and replaced with RPA (0.5 μM for 20 minutes in HBSS [Invitrogen] at 37°C). NRCMs were washed twice with HBSS and incubated for additional 15 minutes in a dye-free buffer. RPA red fluorescence and GFP fluorescence were determined by quantitative laser scanning microscopy from 5 randomly selected fields. Images were quantified by measuring the mean pixel intensity for the RPA fluorescence using ImageJ (NIH). Calculated RPA fluorescence intensities were normalized to the GFP-positive area.

Measurement of ROS. MitoSox Red (Invitrogen), a mitochondrion-specific hydroethidine-derivative fluorescent dye, was used to assess mitochondrial O_2^- production in NRCMs, as previously described (50). After treatment with ABCB8 siRNA or adenovirus, NRCMs were treated with MitoSOX Red (5 μM) in the absence and presence of DOX (10 μM) for 16 hours at 37°C in the dark, washed with PBS, and returned to warm HBSS for imaging. Stained cells were analyzed by quantitative laser scanning microscopy. Gain and amplifier settings were held constant throughout the experiment. DCF fluorescence was assessed by fluorescent microscopy in NRCMs treated with control or ABCB8 siRNA for 48 hours and 10 μM DOX for 16 hours. Cells were washed once with PBS and stained with 5 μM DCF (Molecular Probes) in HBSS for 30 minutes at 37°C in the dark. Following dye loading, cells were washed once with PBS and incubated in complete medium for 10 minutes prior to imaging. DCF fluorescence intensity was quantified by ImageJ software.

Cell viability. Cell viability in NRCMs was assessed by MTS (Cell Titer 96 Aqueous Nonradioactive Cell Proliferation Assay Kit, Promega) according to the manufacturer's protocol. HEK293 cell viability was determined by staining with Annexin V (Invitrogen; early apoptosis), DAPI permeability, or trypan blue permeability (late apoptosis and necrosis). Annexin V– and DAPI-positive cells were quantified by flow cytometry. Trypan blue–positive cells were counted under the light microscope and expressed as percentage of the total. For determination of myocardial apoptosis, frozen heart sections were permeabilized in 0.1% Triton X-100 in PBS containing 0.1% sodium citrate for 2 minutes and washed, and the fluorescent TUNEL (Roche) mixture was added for 60 minutes at 37°C in the dark, followed by counterstaining with DAPI. The number of TUNEL-positive cardiomyocytes was counted in 10 randomly selected high-power fields on the left ventricular free wall. The percentage of TUNEL-positive cardiomyocytes was calculated by dividing the number of TUNEL-positive cardiomyocytes by the total number of nuclei in 10 microscopic fields.

Generation of ABCB8 TG mice. The coding sequence of ABCB8 cDNA was amplified using PCR and ABCB8-GFP plasmid as a template (51). The PCR product was cloned into the TOPO vector (Invitrogen), and the sequence of the entire region was confirmed by sequencing. *Spe*I and *Cla*I restriction sites were engineered in the 5′ and 3′ ends of the PCR product, respectively. A plasmid containing α-MHC promoter and human growth hormone poly(A) sequence was provided by Jeffrey Robbins (Cincinnati Children's Hospital, Cincinnati, Ohio, USA). The ABCB8 fragment was cut out of TOPO, gel isolated, and cloned into this plasmid. The plasmid was purified using the Qiagen EndoFree Plasmid Maxi Kit. The purified plasmid was digested with *Not*I (which flanks the region containing the transgene), and the 10.5-kb fragment has been gel isolated.

The microinjections of the transgene were performed by the Northwestern Transgenic and Targeted Mutagenesis Core Facility, as described previously (52). Potential founder mice (which grew from the injected zygotes) were screened for insertion of the transgene by PCR analysis after DNA was obtained from their tail tip. The screening identified 5 founder mice. We selected one stable TG line, which had a high level of ABCB8 protein expression in the heart, intact fertility, and normal cardiac function for subsequent analyses. This founder mouse was backcrossed 7 times to C57BL/6J mice. Tissue-specific expression patterns and the level of expression were determined by Western blot analysis and qRT-PCR. See complete unedited blots in the supplemental material.

cs-*Abcb8*$^{-/-}$ mice were generated as described previously (17). They were treated with DOX 7 days after PO tamoxifen treatment was completed.

Lipid peroxidation assay. Malondialdehyde (MDA) and 4-hydroxyalkenals (HAE) concentrations were determined spectrophotometrically using a commercially available Lipid Peroxidation Microplate Assay Kit (Oxford Biomedical Research). This assay is based on the reaction of a chromogenic reagent, N-methyl-2-phenylindole, with MDA and HAE, yielding a stable chromophore with maximal absorbance at 586 nm. Freshly isolated heart tissue (~50 mg) was rinsed with cooled PBS and homogenized for 30 seconds in PBS containing 5 mM butylatedhydroxytoluene. The samples were then centrifuged at 3,000 *g* for 10 minutes at 4°C to remove large particles and were mixed with N-methyl-2-phenylindole in acetonitrile and methanesulfonic acid, followed by incubation at 45°C for 60 minutes. Samples were then centrifuged again at 15,000 *g* for 10 minutes, followed by measurement of absorbance at 586 nm.

Echocardiography. Echocardiography was performed using a Vevo 770 High-Resolution Imaging System. Animals were anesthetized with isoflurane and placed in a supine position. The chests were shaved, and the parasternal short- and long-axis views were used to obtain 2-dimensional and M-mode images. At least 10 independent cardiac cycles per each experiment were obtained.

Hemodynamic measurements. A high-fidelity 1.2 Fr transducer-tipped pressure-volume (PV) catheter (Scisense Inc.) was calibrated in 37°C saline and introduced into the left ventricle of the anesthetized mouse to evaluate hemodynamic parameters. The left ventricular apex was exposed by thoracotomy, and the catheter was advanced through the apex to lie along the longitudinal axis. PV data were collected in a steady state. Signals were digitized by use of a data translation series analog-to-digital converter. Values derived from pressure tracings were averaged over a minimum of 20 beats.

Histochemical analysis. Heart tissue was fixed in methanol, embedded in paraffin, and sectioned. To determine cardiac fiber morphology, sections were stained with H&E according to the standard protocols. Heart fibrosis was assessed by Masson trichrome staining.

For analysis of cardiomyocyte size, the middle third of each heart was fixed in methanol and embedded in paraffin. Four-μm-thick sections were stained with H&E, and cardiomyocyte size was measured by light microscopy. Five fields from four heart sections were randomly selected. Sarcolemmal surface area was calculated using ImageJ software (NIH).

Measurement of DOX in cells. The concentration of DOX was determined using spectrophotometric assay (53). DOX absorbance was read at

480 nm from a solution consisting of the sample or standard. Standards were prepared using diluted DOX in the 0.4~100.0 μM range (Supplemental Figure 1). The concentration of DOX in samples was corrected by protein concentration.

DOX, DXZ, and DFO treatment of animals. We treated mice at the age of 8 to 9 weeks with cumulative doses of DOX (30 mg/kg in 3 injections over a period of 5 days [protocol 1] or 24 mg/kg in 4 injections over a period of 10 days [protocol 2] via intraperitoneal administration). In the control group, gender-matched littermate control animals were injected with PBS. Tissues were harvested for subsequent analyses 1 week (protocol 1) or 1 month (protocol 2) after treatment. The animals were observed daily and weighed weekly. Iron chelators were administered by intraperitoneal injections (DFO, 50 mg/kg; DXZ, 60 mg/kg) 2 hours before every DOX injection.

Statistics. Data are expressed as mean ± SEM. A P value of less than 0.05 was considered statistically significant. Statistical significance was assessed with the unpaired 2-tail Student's t test and ANOVA, using SPSS software, for comparisons of more than 2 groups. Use of ANOVA is indicated in figure legends.

Study approval. All animal studies were reviewed and approved by the Northwestern Animal Care and Use Committee, Chicago, Illinois, USA. Nonfailing and failing human heart samples were obtained from the Human Heart Tissue Collection at the Cleveland Clinic. Informed consent was obtained from all the transplant patients and from the families of the organ donors before tissue collection. Protocols for tissue procurement were approved by the Institutional Review Board of the Cleveland Clinic (Cleveland, Ohio, USA), which is AAHRPP accredited.

Acknowledgments

We thank Amy Rines, Aarif Kakhoo, and Jerry Kaplan for their helpful comments. Imaging work was performed at the Northwestern University Cell Imaging Facility, which is supported by the NCI CCSG P30 CA060553 award to the Robert H. Lurie Comprehensive Cancer Center. H. Ardehali is supported by NIH K02 HL107448, R01 HL087149, R01 HL104181, and 1PO1 HL108795.

Received for publication August 30, 2013, and accepted in revised form October 17, 2013.

Address correspondence to: Hossein Ardehali, Tarry 14-733, 303 E. Chicago Ave., Chicago, Illinois 60611, USA. Phone: 312.503.2342; Fax: 312.503.0137; E-mail: h-ardehali@northwestern.edu.

1. Binaschi M, et al. Anthracyclines: selected new developments. Current medicinal chemistry. *Curr Med Chem Anticancer Agents*. 2001;1(2):113–130.
2. Ferrans VJ, Clark JR, Zhang J, Yu ZX, Herman EH. Pathogenesis and prevention of doxorubicin cardiomyopathy. *Tsitologiia*. 1997;39(10):928–937.
3. Jones RL, Swanton C, Ewer MS. Anthracycline cardiotoxicity. *Expert Opin Drug Saf*. 2006;5(6):791–809.
4. Simunek T, Sterba M, Popelova O, Adamcova M, Hrdina R, Gersl V. Anthracycline-induced cardiotoxicity: overview of studies examining the roles of oxidative stress and free cellular iron. *Pharmacol Rep*. 2009;61(1):154–171.
5. Berthiaume JM, Wallace KB. Adriamycin-induced oxidative mitochondrial cardiotoxicity. *Cell Biol Toxicol*. 2007;23(1):15–25.
6. Myers C. The role of iron in doxorubicin-induced cardiomyopathy. *Seminars in oncology*. 1998; 25(4 suppl 10):10–14.
7. Keizer HG, Pinedo HM, Schuurhuis GJ, Joenje H. Doxorubicin (adriamycin): a critical review of free radical-dependent mechanisms of cytotoxicity. *Pharmacol Ther*. 1990;47(2):219–231.
8. Myers CE, Gianni L, Simone CB, Klecker R, Greene R. Oxidative destruction of erythrocyte ghost membranes catalyzed by the doxorubicin-iron complex. *Biochemistry*. 1982;21(8):1707–1712.
9. Xu X, Persson HL, Richardson DR. Molecular pharmacology of the interaction of anthracyclines with iron. *Mol Pharmacol*. 2005;68(2):261–271.
10. Panjrath GS, Patel V, Valdiviezo CI, Narula N, Narula J, Jain D. Potentiation of Doxorubicin cardiotoxicity by iron loading in a rodent model. *J Am Coll Cardiol*. 2007;49(25):2457–2464.
11. Miranda CJ, et al. Hfe deficiency increases susceptibility to cardiotoxicity and exacerbates changes in iron metabolism induced by doxorubicin. *Blood*. 2003;102(7):2574–2580.
12. Hasinoff BB, Herman EH. Dexrazoxane: how it works in cardiac and tumor cells. Is it a prodrug or is it a drug? *Cardiovasc Toxicol*. 2007;7(2):140–144.
13. Swain SM, Vici P. The current and future role of dexrazoxane as a cardioprotectant in anthracycline treatment: expert panel review. *J Cancer Res Clin Oncol*. 2004;130(1):1–7.
14. Herman EH, Ferrans VJ. Examination of the potential long-lasting protective effect of ICRF-187 against anthracycline-induced chronic cardiomyopathy. *Cancer Treat Rev*. 1990;17(2–3):155–160.
15. Xu X, Persson HL, Richardson DR. Molecular pharmacology of the interaction of anthracyclines with iron. *Mol Pharmacol*. 2005;68(2):261–271.
16. Higgins CF, Linton KJ. ABC transporters: An introduction and overview. In: Holland IB, Cole SP, Kuchler K, Higgins CF, eds. *ABC Proteins: From Bacteria to Man*. San Diego, California, USA: Academic Press; 2003:xvii-xxii.
17. Ichikawa Y, et al. Disruption of ATP-binding cassette B8 in mice leads to cardiomyopathy through a decrease in mitochondrial iron export. *Proc Natl Acad Sci U S A*. 2012;109(11):4152–4157.
18. Hasinoff BB, Schnabl KL, Marusak RA, Patel D, Huebner E. Dexrazoxane (ICRF-187) protects cardiac myocytes against doxorubicin by preventing damage to mitochondria. *Cardiovasc Toxicol*. 2003; 3(2):89–99.
19. Sarvazyan N. Visualization of doxorubicin-induced oxidative stress in isolated cardiac myocytes. *Am J Physiol*. 1996;271(5 pt 2):H2079–H2085.
20. Marechal X, et al. Doxorubicin-induced cardiac dysfunction is attenuated by ciclosporin treatment in mice through improvements in mitochondrial bioenergetics. *Clin Sci (Lond)*. 2011;121(9):405–413.
21. Clementi ME, Giardina B, Di Stasio E, Mordente A, Misiti F. Doxorubicin-derived metabolites induce release of cytochrome C and inhibition of respiration on cardiac isolated mitochondria. *Anticancer Res*. 2003;23(3B):2445–2450.
22. Kwok JC, Richardson DR. Unexpected anthracycline-mediated alterations in iron-regulatory protein-RNA-binding activity: the iron and copper complexes of anthracyclines decrease RNA-binding activity. *Mol Pharmacol*. 2002;62(4):888–900.
23. Minotti G, Ronchi R, Salvatorelli E, Menna P, Cairo G. Doxorubicin irreversibly inactivates iron regulatory proteins 1 and 2 in cardiomyocytes: evidence for distinct metabolic pathways and implications for iron-mediated cardiotoxicity of antitumor therapy. *Cancer Res*. 2001; 61(23):8422–8428.
24. Petrat F, Weisheit D, Lensen M, de Groot H, Sustmann R, Rauen U. Selective determination of mitochondrial chelatable iron in viable cells with a new fluorescent sensor. *Biochem J*. 2002; 362(pt 1):137–147.
25. Rauen U, et al. Assessment of chelatable mitochondrial iron by using mitochondrion-selective fluorescent iron indicators with different iron-binding affinities. *Chembiochem*. 2007;8(3):341–352.
26. Elihu N, Anandasbapathy S, Frishman WH. Chelation therapy in cardiovascular disease: ethylenediaminetetraacetic acid, deferoxamine, and dexrazoxane. *J Clin Pharmacol*. 1998;38(2):101–105.
27. Hoyes KP, Porter JB. Subcellular distribution of desferrioxamine and hydroxypyridin-4-one chelators in K562 cells affects chelation of intracellular iron pools. *Br J Haematol*. 1993;85(2):393–400.
28. Ihnat PM, Vennerstrom JL, Robinson DH. Synthesis and solution properties of deferoxamine amides. *J Pharm Sci*. 2000;89(12):1525–1536.
29. Lipshultz SE, et al. Assessment of dexrazoxane as a cardioprotectant in doxorubicin-treated children with high-risk acute lymphoblastic leukaemia: long-term follow-up of a prospective, randomised, multicentre trial. *Lancet Oncol*. 2010;11(10):950–961.
30. Zhang S, et al. Identification of the molecular basis of doxorubicin-induced cardiotoxicity. *Nat Med*. 2012; 18(11):1639–1642.
31. Rao VA. Iron chelators with topoisomerase-inhibitory activity and their anticancer applications. *Antioxid Redox Signal*. 2013;18(8):930–955.
32. Lyu YL, et al. Topoisomerase IIbeta mediated DNA double-strand breaks: implications in doxorubicin cardiotoxicity and prevention by dexrazoxane. *Cancer Res*. 2007;67(18):8839–8846.
33. Andoh T, Ishida R. Catalytic inhibitors of DNA topoisomerase II. *Biochim Biophys Acta*. 1998;1400(1–3):155–171.
34. Hasinoff BB, Abram ME, Barnabé N, Khélifa T, Allan WP, Yalowich JC. The catalytic DNA topoisomerase II inhibitor dexrazoxane (ICRF-187) induces differentiation and apoptosis in human leukemia K562 cells. *Mol Pharmacol*. 2001;59(3):453–461.
35. Neufeld EJ. Update on iron chelators in thalassemia. Hematology / the Education Program of the American Society of Hematology. American Society of Hematology. *Education Program*. 2010;2010:451–455.
36. Herman EH, Zhang J, Ferrans VJ. Comparison of the protective effects of desferrioxamine and ICRF-187 against doxorubicin-induced toxicity in spontaneously hypertensive rats. *Cancer Chemother Pharmacol*. 1994;35(2):93–100.
37. Hershko C, et al. Anthracycline toxicity is potentiated by iron and inhibited by deferoxamine: studies in rat heart cells in culture. *The J Lab Clin Med*. 1993; 122(3):245–251.
38. Zanninelli G, et al. Chelation and mobilization of cellular iron by different classes of chelators. *Mol Pharmacol*. 1997;51(5):842–852.
39. Hasinoff BB, Patel D, Wu X. The oral iron chelator

ICL670A (deferasirox) does not protect myocytes against doxorubicin. *Free Radic Biol Med*. 2003;35(11):1469–1479.
40. Popelova O, et al. Deferiprone does not protect against chronic anthracycline cardiotoxicity in vivo. *J Pharmacol Exp Ther*. 2008;326(1):259–269.
41. Kwok JC, Richardson DR. Anthracyclines induce accumulation of iron in ferritin in myocardial and neoplastic cells: inhibition of the ferritin iron mobilization pathway. *Mol Pharmacol*. 2003;63(4):849–861.
42. Xu X, Sutak R, Richardson DR. Iron chelation by clinically relevant anthracyclines: alteration in expression of iron-regulated genes and atypical changes in intracellular iron distribution and trafficking. *Mol Pharmacol*. 2008; 73(3):833–844.
43. Rao VA. Iron chelators with topoisomerase-inhibitory activity and their anticancer applications. *Antioxid Redox Signal*. 2013;18(8):930–955.
44. Martin E, et al. Evaluation of the topoisomerase II-inactive bisdioxopiperazine ICRF-161 as a protectant against doxorubicin-induced cardiomyopathy. *Toxicology*. 2009;255(1–2):72–79.
45. Swain SM, et al. Cardioprotection with dexrazoxane for doxorubicin-containing therapy in advanced breast cancer. *J Clin Oncol*. 1997;15(4):1318–1332.
46. Tebbi CK, et al. Dexrazoxane-associated risk for acute myeloid leukemia/myelodysplastic syndrome and other secondary malignancies in pediatric Hodgkin's disease. *J Clin Oncol*. 2007; 25(5):493–500.
47. Salzer WL, et al. Long-term results of the pediatric oncology group studies for childhood acute lymphoblastic leukemia 1984-2001: a report from the children's oncology group. *Leukemia*. 2010;24(2):355–370.
48. MHRA. Dexrazoxane (Cardioxane): restriction of use to adults with advanced or metastatic breast cancer only. *Drug Safety Update*. 2011;4(12):A3.
49. Tangeras A, Flatmark T, Backstrom D, Ehrenberg A. Mitochondrial iron not bound in heme and iron-sulfur centers. Estimation, compartmentation and redox state. *Biochim Biophys Acta*. 1980; 589(2):162–175.
50. Gordon LI, et al. Blockade of the erbB2 receptor induces cardiomyocyte death through mitochondrial and reactive oxygen species-dependent pathways. *J Biol Chem*. 2009;284(4):2080–2087.
51. Ardehali H, Xue T, Dong P, Machamer C. Targeting of the mitochondrial membrane proteins to the cell surface for functional studies. *Biochem Biophys Res Commun*. 2005;338(2):1143–1151.
52. Albert Y, Whitehead J, Eldredge L, Carter J, Gao X, Tourtellotte WG. Transcriptional regulation of myotube fate specification and intrafusal muscle fiber morphogenesis. *J Cell Biol*. 2005;169(2):257–268.
53. Mayer LD, Hope MJ, Cullis PR, Janoff AS. Solute distributions and trapping efficiencies observed in freeze-thawed multilamellar vesicles. *Biochim Biophys Acta*. 1985;817(1):193–196.